Monovalent and Divalent Cation Permeation in Acetylcholine Receptor Channels

Ion Transport Related to Structure

JOHN A. DANI and GEORGE EISENMAN

From the Section of Molecular Neurobiology, Yale University School of Medicine, New Haven, Connecticut 06510, and the Department of Physiology, University of California at Los Angeles School of Medicine, Los Angeles, California 90024

ABSTRACT Single channel patch-clamp techniques were used to study nicotinic acetylcholine receptors in cultured rat myotubes. The single channel conductance in pure cesium and sodium levels off at high concentrations, as if a binding site within the channel were saturating. The conductances at very low concentrations, however, are larger than predicted by the simplest one-site transport model fitted to the high-concentration data. At low concentrations, the current-voltage relations are inwardly rectifying, but they become more ohmic if a small amount of divalent cations is added externally. Magnesium and barium are good permeants that have rather high affinities for the channel. Upon adding low millimolar concentrations of these divalent cations externally to a membrane bathed in pure cesium, the inward current carried by cesium is decreased. As more divalent cations are added, the inward-going currents continued to decrease and the divalent cation replaces cesium as the main current carrier. The ion transport data are described by considering the size, shape, and possible net charge of the channel. In that way, even the complex features of transport are explained in a realistic physical framework. The results are consistent with the channel having long, wide, multiply occupied vestibules that serve as transition zones to the short, selective, singly occupied narrow region of the channel. A small amount of net negative charge within the pore could produce concentration-dependent potentials that provide a simple explanation for the more complicated aspects of the permeation properties.

INTRODUCTION

Nicotinic acetylcholine (ACh) receptors are concentrated at the vertebrate neuromuscular junction, at synapses on autonomic ganglion cells, and at synapses in the central nervous system; extrasynaptic receptors appear diffusely on embryonic, uninnervated, and denervated muscle cells. At synapses, ACh receptors bind ACh released by the presynaptic neuron and undergo a conformational

Address reprint requests to Dr. John A. Dani, Section of Molecular Neurobiology, Tompkins 5, Yale University School of Medicine, 333 Cedar St., P.O. Box 3333, New Haven, CT 06510.

J. GEN. PHYSIOL. © The Rockefeller University Press · 0022-1295/87/06/0959/25$1.00

Volume 89 June 1987 959–983

change that opens ionic channels responsible for depolarizing the postsynaptic cell.

Previous work has established that the ACh receptor channel is an aqueous pore that selects against anions but passes many nonelectrolytes and cations <0.8 nm in diameter (Takeuchi and Takeuchi, 1960; Huang et al., 1978; Dwyer et al., 1980; Adams et al., 1980). Ions do not move through the channel independently; instead, there is competitive binding within the pore (Lewis, 1979; Dwyer et al., 1980; Adams et al., 1981; Sanchez et al., 1986). In addition, reversal potential measurements and current fluctuation analysis have shown that small inorganic divalent cations are permeants that decrease the conductance of monovalent cations (Bregestovshi et al., 1979; Lewis, 1979; Marchais and Marty, 1979; Adams et al., 1980; Magleby and Weinstock, 1980; Takeda et al., 1982).

Some of the ion transport data can be described by assuming that a cation encounters an energy profile within the pore that has one site between two barriers. This simple two-barrier, one-site Eyring rate theory model, however, has shortcomings: it cannot adequately describe reversal potentials in mixtures of monovalent and divalent cations (Lewis and Stevens, 1979), it cannot at the same time explain both conductance and current block (Adams et al., 1981; Dwyer and Farley, 1984), and it cannot describe the concentration dependence of currents carried by organic cations (Sanchez et al., 1986).

The purpose of this study is to provide ion transport data over a wide concentration and voltage range in a variety of solutions. Current-voltage (*I-V*) relations in simple solutions that contain only one monovalent electrolyte provide transport information in the absence of interaction with another electrolyte or nonelectrolyte. The *I-V* relations are asymmetric and inwardly rectifying at low concentrations, and the shape of the *I-V* relation changes with concentration. Although the single channel conductance is not a simple function of concentration, the conductance does level off at high concentrations, as if a single site in the narrow region of the channel were becoming saturated. These monovalent *I-V* relations define the basic properties of the channel and allow the effects of low concentrations of added divalent cations to be determined. Magnesium and barium are permeants that carry significant current. These divalent cations have a higher affinity for the channel than the monovalent cations we studied. Therefore, when present, these divalent cations decrease the current carried by cesium, and they can displace cesium as the main current carrier at higher concentrations. Finally, structural and biochemical information is used to develop a simple ion transport model (Dani, 1986*a*) that can quantitatively describe the results. A two-barrier, one-site rate theory model is used to describe the narrow region of the channel, and wide-entrance vestibules with net negative charge explain other aspects of transport in a physically realistic manner.

Taken together, the *I-V* relations provide a sensitive assay of the ion transport properties of the channel. The complete data set is intended to serve as a basis to guide future quantitative descriptions of ion permeation using molecular or Brownian dynamics (Mackay et al., 1984; Cooper et al., 1985). The *I-V* relations also provide the data base needed for relating structure and function and for analyzing the functional changes that result from site-directed mutagenesis of

the cloned subunit cDNA (Mishina et al., 1985). Preliminary reports of this work have been presented at meetings (Dani and Eisenman, 1984, 1985; Eisenman and Dani, 1986).

METHODS

Patch-clamp techniques were used to obtain gigohm seals on cultured rat myotubes to measure single channel ACh receptor currents over a wide range of electrolyte concentrations and membrane potentials.

Tissue Culture

About 2 g of skeletal muscle was dissected from the hind legs of newborn rats. The muscle was minced and then stirred slowly in 45 ml of divalent-free phosphate-buffered saline containing 0.0025% trypsin. At roughly 20-min intervals, 10 ml of supernatant was pipetted into centrifuge tubes containing 0.75 ml horse serum, and 10 ml more of the trypsin solution was added to the tissue incubation until the dissociation was complete. The cells were centrifuged at 200 *g* for 10 min, and the pellets were resuspended in the growth medium: Dulbecco's modified Eagle's medium, 10% horse serum, 1% chick embryo extract, 100 U/ml penicillin, and 100 μg/ml streptomycin (all from Gibco, Grand Island, NY). The cells were preplated to decrease the fraction of fibroblasts: the cells were grown overnight in a flask, transferred to another flask for 30 min, and then plated onto coverslips. The coverslips were pretreated in one of three ways to make the myoblasts stick better: (*a*) fibroblasts were grown on the coverslips and then lysed in distilled water, or (*b*) the coverslips were coated with collagen, or (*c*) the coverslips were coated with a mixture of collagen and poly-D-lysine. The cells were maintained at 36°C in a humidified atmosphere of 10% CO_2 and 90% air. After the myoblasts began to fuse, the cultures were treated with 10 μM D-arabinofuranosylcytosine for 2 or 3 d to inhibit fibroblast growth. The myotubes were used 7–14 d after the initial plating.

Patch-Clamp Techniques

Single channel ACh receptor currents were measured using standard patch-clamp techniques (Hamill et al., 1981; Sakmann and Neher, 1983). Following the suggestion of Rae and Levis (1984), patch pipettes were pulled in two stages from Kovar 7052 glass (Corning Glass Works, Corning, NY) and then coated with polystyrene Q-dope (GC Electronics, Rockford, IL). The tips of the pipettes were fire-polished by a hot platinum wire coated with Kovar glass (Dani and Eisenman, 1984).

In the vast majority of cases, outside-out membrane patches were used. After a patch was excised, it was placed deep into an inflow port of the external test solution that contained 0.1–0.6 μM ACh to induce single ACh receptor channel openings. Placing the patch deep into the inflow port ensured a complete solution change, and the slow flow of solution did not introduce noise or disturb the patch. Holding potentials and voltage ramps were applied with a programmable stimulator (Page-10, Page Electronics, Duarte, CA) or a waveform generator (model F53A, Interstate Electronics Corp., Anaheim, CA). The currents were recorded across a 10-G resistor of a conventional patch clamp (Sakmann and Neher, 1983), low-pass-filtered at 600–1,000 Hz by an eight-pole Bessel filter (LPF 902, Frequency Devices, Haverhill, MA), digitally sampled every 0.2 ms with a 12-bit analog-to-digital converter controlled by a PDP 11/34 computer (Digital Equipment Corp., Marlboro, MA), and saved on a floppy disk. Only the dominant unitary-current step size was analyzed, and in most patches, other current step sizes were very rare or absent. In addition, current events had to last for at least three sample intervals and be

unquestionable channel events before they were included in the averaging used to create the current-voltage relation. The measurements were made at room temperature, which was held at 21 ± 1°C.

Although analog capacitance and leakage correction was used, when voltage ramps were applied to the patch, it was necessary to correct the single channel current records precisely by subtracting averaged baselines in the absence of channel openings from the record containing the event. Fig. 1 illustrates the way in which many corrected single channel current segments were combined at each voltage and averaged by computer to

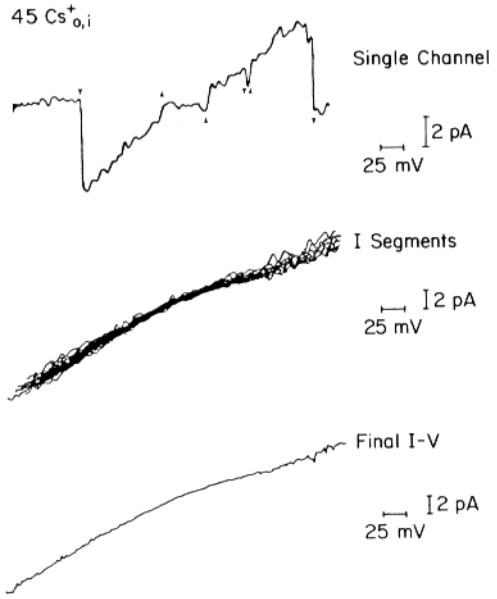

FIGURE 1. This illustrates the steps in creating an *I-V* relation from single channel currents. The upper leak-corrected single channel record shows several ACh receptor channel openings, labeled by arrows, that occurred as the voltage was ramped from −200 to +200 mV. Many single channel current segments were isolated by computer and are shown together in the middle *I-V* relation. The current segments were averaged at each voltage to obtain the final *I-V* relation. Note that the shape of the *I-V* relation is preserved from the single channel event to the final *I-V*.

obtain the final *I-V* relation. Each *I-V* was standardized to have a current represented every 2 mV and, if necessary, the zero-current potential was adjusted so that *I-V* relations from different patches in the same solutions could be combined without introducing scatter. Since the zero-current potentials varied by a few millivolts among equivalent patches, the currents from each patch were shifted along the voltage axis to make their zero-current potential coincide with the theoretical value expected from the bathing solutions. The zero-current potential in symmetrical solutions must, by definition, occur at 0 mV, and extra experiments were performed in asymmetrical solutions to determine the reversal potential directly, as well as to account for liquid junction potentials.

When necessary, liquid junction potentials were measured between a pipette filled with 3 M KCl and the Ag/AgCl bath electrode using the tracking circuit of the patch clamp.

The solutions and the configuration of the set-up exactly duplicated the way the experiments were performed. The pipette was moved from the bath solution into the solution in the inflow port. The liquid junction potential was measured for various lengths of time to check whether the solution from the inflow port altered the bath enough to change the potential as a function of time. Also, the potential was measured with or without slight pressure applied to the 3 M KCl pipette to test whether mixing at the pipette tip altered the measurement. In all cases, the liquid junction potential maintained a consistent value that did not vary significantly.

Solutions

Table I lists the solutions that the patches were exposed to after they were placed into the inflow port. Cesium salts were obtained from Alfa Products, Danvers, MA; other salts were from J. T. Baker Chemical Co., Phillipsburg, NJ. During the experiments, the solutions bathing the two sides of the patch were isotonic. The external solutions had chloride as the anion. The cytoplasmic experimental solutions had fluoride as the main anion with at least millimolar amounts of chloride, so the Ag/AgCl electrodes gave stable, defined potentials. The fluoride in the cytoplasmic solutions ensured that the divalent activities were micromolar or less; the fluoride on the inside seemed to give more stable patches. The experiments with cesium had no divalent cations or nonelectrolyte added, except in the case of 7 mM cesium, where 298 mM sucrose was present. Divalent cation chelating agents were not added to the external solutions. In the experiments with sodium, $\leq$1 mM $BaCl_2$ was occasionally added, but there was no nonelectrolyte. When mixtures of cesium and divalent cations were being studied, the solutions were made isotonic with sucrose.

The composition of the bath solution was made very similar to the solution in the patch pipette so that the bath would not contaminate the pipette solution during the formation of a patch. The concentration of the main ion in the bath was set equal to that in the pipette, millimolar amounts of divalent cations were added, and the tonicity of the bath was made equal to that of the myotubes by adding sucrose. Although the cytoplasm and bath were isotonic and the solutions bathing both sides of the excised patch in the inflow port were isotonic, the patch pipette and bath were often not isotonic. Since, to eliminate possible artifacts, the patch pipette osmolarity often did not match the bath and the solutions bathing the patch did not contain divalent ions, many attempts were necessary before an acceptable, very stable seal was obtained that could withstand the protocol and the high applied voltages.

Ionic activities in pure solutions were calculated from tables of mean activity coefficients (Robinson and Stokes, 1959; Weast and Astle, 1978–1979). In addition, measurements to determine the activities in mixtures were made with electrodes specific for monovalent cations (476220, Corning Glass Works), divalent cations (933200, Orion Research, Cambridge, MA), and chloride (using Ag/AgCl). A calomel, saturated KCl fiber-junction electrode was used as the reference, and the voltages were measured with a digital pH meter. Pure solutions of cesium chloride, sodium chloride, magnesium chloride, and barium chloride served as standards. The final activities of the mixtures were estimated by comparing the ion-specific potentials of the mixtures with the potentials of the pure solutions whose activities were obtained from the tables. The general results of the measurements with the ion-specific electrodes are as follows. The sucrose used to maintain isotonicity had no significant effect on the activities. The 45 mM cesium chloride present in the external solution mixtures had very little effect on the activities of magnesium chloride or barium chloride. The divalent ions, however, decreased the activity of cesium in the mixtures.

TABLE I

Main permeant activity	Inside concentration	Outside concentration
mM	*mM*	*mM*
6.9 $Cs_{i,o}$	5.6 CsF	7.0 CsCl
	1.4 CsCl	
	0.1 $MgCl_2$*	
	0.05 $CaCl_2$	
	0.5 EGTA	
	1.0 HEPES‡	1.0 HEPES
	298.0 sucrose	298.0 sucrose
18.2 $Cs_{i,o}$	16.0 CsF	20.0 CsCl
	4.0 CsCl	
	0.3 $MgCl_2$	
	0.1 $CaCl_2$	
	1.5 EGTA	
	2.0 HEPES	2.0 HEPES
39.3 $Cs_{i,o}$	45.0 CsF	45.0 CsCl
	0.5 $MgCl_2$	
	0.3 $CaCl_2$	
	4.5 EGTA	
	5.0 HEPES	5.0 HEPES
110.6 $Cs_{i,o}$	150.0 CsF	150.0 CsCl
	2.0 $MgCl_2$	
	1.0 $CaCl_2$	
	11.0 EGTA	
	5.0 HEPES	5.0 HEPES
200.3 $Cs_{i,o}$	200.0 CsF	300.0 CsCl
	100.0 CsCl	
	5.0 HEPES	5.0 HEPES
39.2 $Na_{i,o}$	45.0 NaF§	45.0 NaCl
		0.5 $BaCl_2$‖
	5.0 HEPES	5.0 HEPES
115.0 $Na_{i,o}$	150.0 NaF	150.0 NaCl
		0.5 $BaCl_2$
	5.0 HEPES	5.0 HEPES
312.0 $Na_{i,o}$	450.0 NaCl	450.0 NaCl
	5.0 HEPES	5.0 HEPES
0.9 Mg_o	40.0 CsF	1.0 $MgCl_2$
39.2 Cs_o	5.0 CsCl	45.0 CsCl
	0.4 $MgCl_2$	
39.3 Cs_i	0.2 $CaCl_2$	
	4.0 EGTA	
	5.0 HEPES	5.0 HEPES
	210.0 sucrose	210.0 sucrose

TABLE I (*continued*)

Main permeant activity	Inside concentration	Outside concentration
mM	*mM*	*mM*
7.5 Mg_o	Same as above	10.0 $MgCl_2$
36.0 Cs_o		45.0 CsCl
		5.0 HEPES
39.3 Cs_i		180.0 sucrose
43.9 Mg_o	Same as above	77.0 $MgCl_2$
30.0 Cs_o		45.0 CsCl
39.3 Cs_i		5.0 HEPES
57.6 Mg_o	Same as above except for 300 sucrose	110.0 $MgCl_2$
29.0 Cs_o		45.0 CsCl
39.3 Cs_i		
		5.0 HEPES
43.9 Mg_o	Same as above	77.0 $MgCl_2$
39.3 Cs_i		5.0 HEPES
		90.0 sucrose
57.6 Mg_o	Same as above	110.0 $MgCl_2$
39.3 Cs_i		5.0 HEPES
0.9 Ba_o	Same as above	1.0 $BaCl_2$
39.1 Cs_o		45.0 CsCl
		5.0 HEPES
39.3 Cs_i		210.0 sucrose
7.4 Ba_o	Same as above	10.0 $BaCl_2$
35.0 Cs_o		45.0 CsCl
		5.0 HEPES
39.3 Cs_i		180.0 sucrose
41.6 Ba_o	Same as above	77.0 $MgCl_2$
29.0 Cs_o		45.0 CsCl
39.9 Cs_i		5.0 HEPES

* Because the solubility product of the MgF_2 and CaF_2 is low, the amount of free divalent in the internal solutions is micromolar or less.

‡ The pH of all the solutions was adjusted to 7.4 with the hydroxide salt of the main permeant. This addition was accounted for in determining the permeant concentration, but the concentration of anions is slightly different from that listed.

§ Outside-out patches were used for all the experiments except those in 45 and 150 mM sodium. Thus, the electrodes were exposed to chloride even though the inflow port contained only fluoride as the anion.

‖ The presence of divalent cations was accounted for during the modeling.

RESULTS

Validity of the Methods

The Methods section describes how the obvious sources of error were avoided when analyzing single channel currents: short openings that were not fully resolved were not used, heterogeneity among the single channels was avoided

by accepting only the dominant conductance state, and capacitance and leakage correction was used. To be certain the ramping procedure did not introduce artifacts, *I-V* relations constructed by measuring single channel currents at different holding potentials were compared with *I-V* relations constructed by applying voltage ramps. This test was intended to check for other possible sources of artifacts. For instance, since the ramps often went from −200 to +200 mV in only 51 ms, it seemed possible that the permeant concentrations next to the

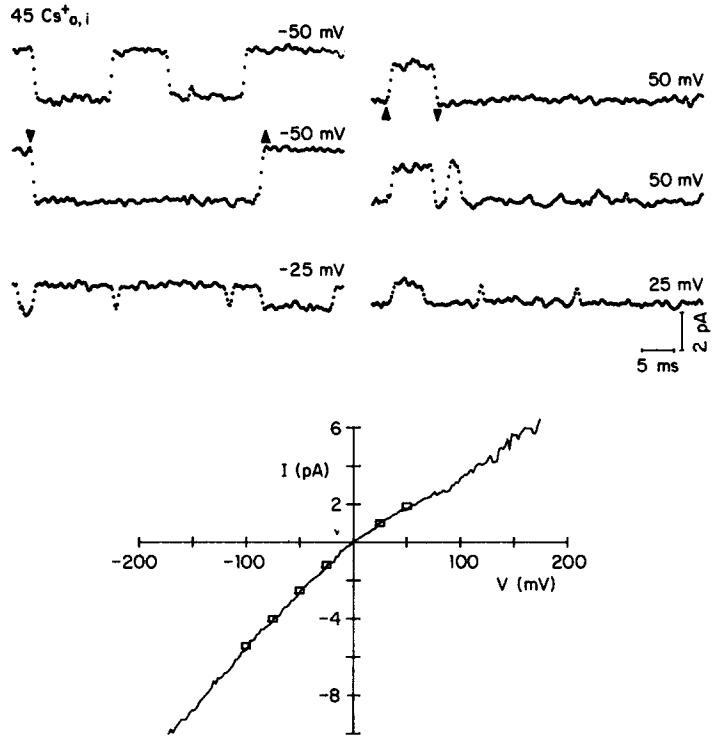

FIGURE 2. Single channel currents and *I-V* relations obtained with 45 mM cesium as the permeant on both sides of the membrane. These single channel currents at the labeled holding potentials show that the inward currents at negative potentials are larger than the outward currents at equivalent positive potentials. The noisy *I-V* was constructed from voltage ramps, and the open squares represent currents obtained at holding potentials. Over the voltage tested, voltage ramps and holding potentials produced the same *I-V* relation.

channel could be altered in a manner that was dependent on the size and speed of the voltage ramp. If the ramp altered the concentration gradients, then the resulting *I-V* relation would not properly reflect the properties of the channel. The bottom of Fig. 2 shows that, over the voltage range tested, the *I-V* relation was the same whether it was constructed using voltage ramps or holding potentials. The noisy, solid *I-V* curve in Fig. 2 was constructed by applying voltage ramps and the overlying open squares are currents obtained at the indicated holding potentials shown in the upper part of the figure.

Because the membrane can survive only brief exposures to large potentials, the currents can be measured over a wider voltage range by using fast ramps. Even though the voltage ranges are not the same, these results suggest the validity of the voltage-ramping technique for determining the shape of *I-V* relations, as has been done for other channels (Yellen, 1984; Eisenman et al., 1986).

In some experiments, sucrose was used to adjust the osmolarity of the solutions. It is known that sucrose and other nonelectrolytes can alter ion transport, for example, by changing the viscosity of the solution or by blocking the channel (Andersen, 1983). Since the ACh receptor channel has a large enough entrance to accommodate sucrose and the channel is permeable to smaller nonelectrolytes (Huang et al., 1978), it is possible that sucrose may not be completely inert. Fig. 3 shows *I-V* relations obtained with symmetrical 20 mM cesium as the permeant with and without 260 mM sucrose present. Over the limited voltage range

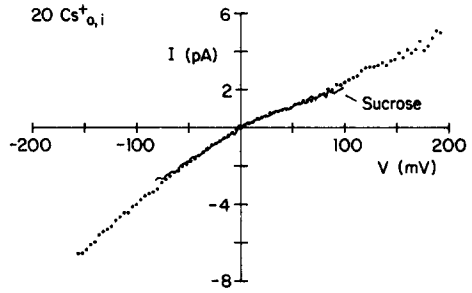

FIGURE 3. The dotted *I-V* relation was obtained with pure, symmetrical 20 mM cesium as the permeant. The solid *I-V* also had 260 mM sucrose added to the solutions. Over the voltage range tested, the sucrose does not significantly alter the *I-V* shape.

studied, the *I-V* relations are similar, which indicates that sucrose causes negligible distortion of the *I-V* relations. With the exception of the *I-V* relation obtained with 7 mM cesium as the permeant, all the actual experiments required less sucrose than was used in this test.

Qualitative Features of the Data

I-V shapes. Fig. 4 shows *I-V* relations in three pure, symmetrical cesium solutions and two pure, symmetrical sodium solutions. The *I-V* shapes are not perfectly ohmic. Rather, they are inwardly rectifying at low concentrations, and they become more ohmic at higher concentrations.

Conductance. Fig. 5 illustrates that, for both cesium and sodium, as the electrolyte concentration increases, the single channel conductance rises and then begins to level off. The simplest way to explain why the conductance levels off is to assume that an ion-binding site within the channel becomes saturated. If the conductance can be described by a rectangular hyperbola on a conductance vs. activity plot (i.e., by Michaelis-Menten kinetics), then ion permeation can be described by a single ion-binding site. The higher-concentration data in Fig. 5 can be described by Michaelis-Menten kinetics, but it is possible that the con-

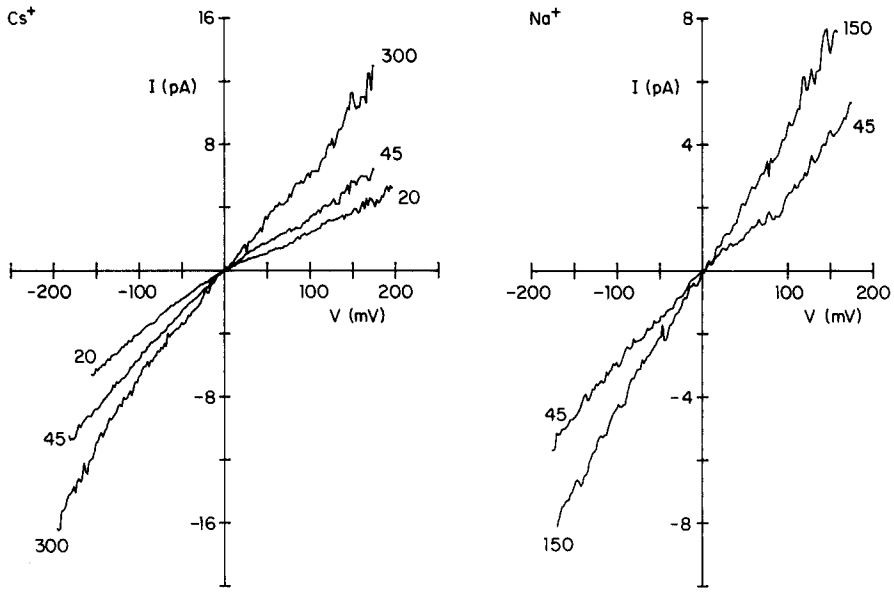

FIGURE 4. Plots of *I-V* relations in pure, symmetrical solutions of cesium or sodium. The concentration of the solutions is indicated in millimolar next to each *I-V* relation. As shown in Table I, 0.5 mM barium was added to the external solution in 45 mM sodium and that may have made the *I-V* relation in 45 mM sodium more linear.

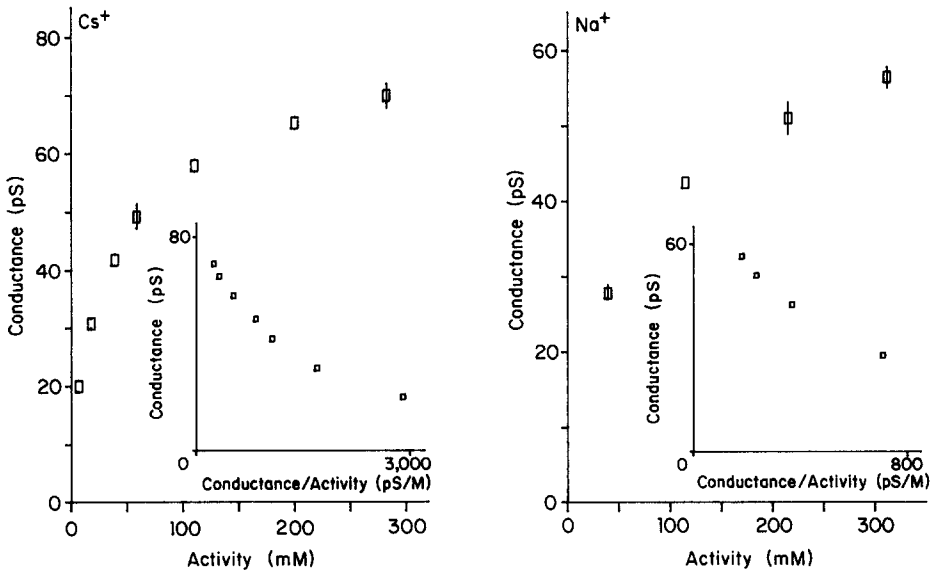

FIGURE 5. Zero-voltage conductance plotted against electrolyte activity in pure, symmetrical cesium and sodium solutions. The insets are Eadie-Hofstee plots. The convex curvature of the inset plots indicates that the conductances at low concentrations are larger than would be predicted by a simple, single-site transport model.

ductance could either resume increasing or even decrease at very high concentrations not studied here. The conductance at low concentrations, however, is larger than predicted by a rectangular hyperbola fitted to the high-concentration data.

The large conductances at low concentrations show up as a deviation from a straight line in the Eadie-Hofstee plot insets of Fig. 5. Usually a curvature in this type of plot is thought to result because there is more than one nonequivalent ion-binding site (Eisenman et al., 1978; Hille and Schwarz, 1978) or because the ion encounters time-dependent energy barriers that fluctuate while the ion moves through the pore (Lauger et al., 1980; Eisenman and Dani, 1986). An alternative explanation is that net negative charge near or within the channel attracts cations to the pore, especially if the bulk electrolyte concentration is low (Dani, 1986*a*). By attracting cations to the pore in a concentration-dependent manner, the negatively charged residues can produce conductances that are surprisingly large at low concentrations. (A general surface charge on the lipid could also produce large conductances at low concentrations if the channel opening were near the membrane surface [Apell et al., 1979; Bell and Miller, 1984]. In the case of the ACh receptor, however, the channel entrance is ~7 nm from the surface of the membrane. Therefore, even if a potential caused by the lipid existed, it would not be expected to influence the ion concentrations or ion transport significantly at such a long distance. In addition, to theoretically introduce such a potential, it would be necessary to have the charge density on the lipid be a completely unknown, adjustable parameter. The differences between the "charged-channel model" used in this article and a general surface charge are discussed by Dani [1986*a*].)

Divalent cations. The single channel currents in Fig. 6 show that divalent cations are permeants that can decrease the current carried by monovalent cations and that divalent cations have a relatively high affinity for the channel. These features can be seen more clearly in Fig. 7.

The dotted *I-V* relation in Fig. 7*A* was obtained with pure, symmetrical 45 mM cesium as the permeant. The solid *I-V* relations show that when either 1 mM magnesium or 1 mM barium is added to the external solution, the inward current is substantially reduced in a voltage-dependent manner. Thus, it seems apparent that these divalent cations enter the pore and influence cesium transport even at submillimolar concentrations. Fig. 7*B* shows *I-V* relations in high external magnesium concentrations. Both of the *I-V* relations in Fig. 7*B* were obtained with 110 mM magnesium outside and 45 mM cesium inside. In addition, the solid *I-V* relation also has 45 mM cesium outside. Adding 45 mM cesium to the 110 mM magnesium in the external solution has very little effect. This result indicates that magnesium is carrying the inward-going current and, at this concentration, magnesium prevents cesium from carrying much inward current. A straightforward explanation of these findings is that divalent cations have a higher affinity for the channel than monovalent cations do. Therefore, as the divalent cation concentration is increased, divalents competitively displace monovalents from the ion-binding site in the pore.

Since divalent cations have a relatively high affinity for the ACh receptor channel, even low concentrations of divalent cations cannot be overlooked when

interpreting monovalent cation transport (see Dani, 1986*a*). Fig. 8 demonstrates how monovalent *I-V* relations may be misinterpreted if the effects of divalent cations are not taken into account. Fig. 8*A* shows the *I-V* relation with pure, symmetrical 45 mM cesium as the permeant and, to convey the shape, a straight

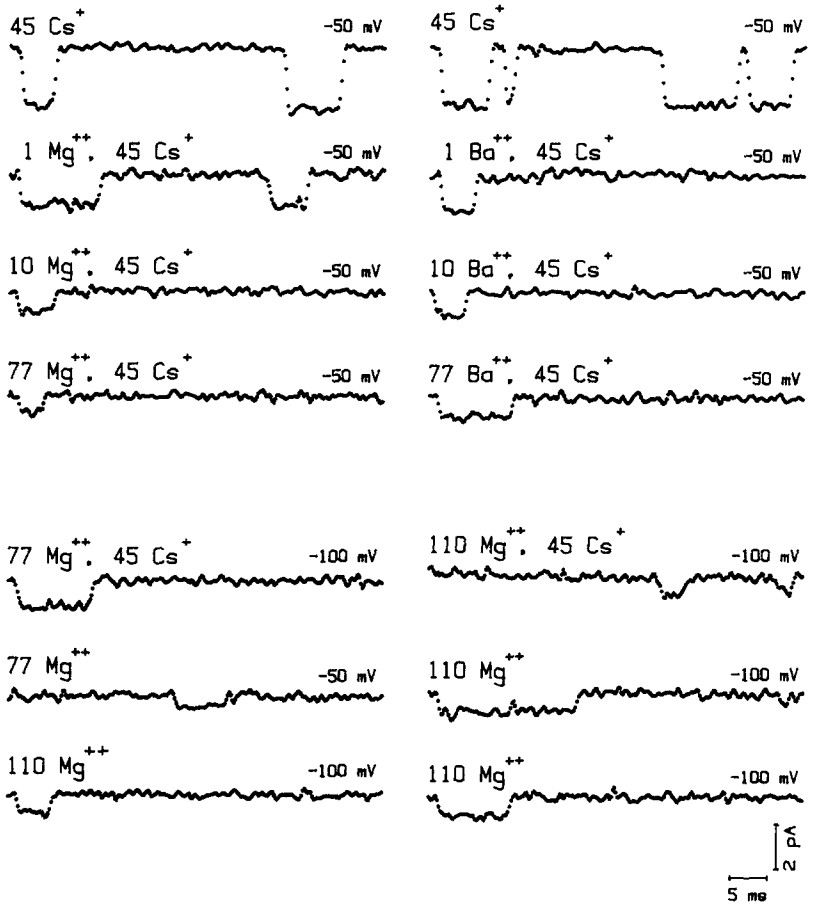

FIGURE 6. These single channel currents demonstrate that magnesium and barium are permeants that decrease the current carried by monovalent cations. The holding potential and the permeants in the external solution are listed next to each record. The permeant bathing the inner surface of the membrane was always 45 mM cesium. When magnesium or barium was added to the 45 mM cesium in the external solution, the inward-going currents decreased. External solutions of pure 77 mM or 110 mM magnesium showed inward-going currents that were carried by magnesium.

line is shown with a slope equal to the zero-voltage conductance of 41.8 pS. Fig. 8*B* shows that when 1 mM barium is added to the external solution, the *I-V* relation appears to become linear and the zero-voltage conductance falls to 36.0 pS. In addition to this dramatic influence on the shape of monovalent cation *I-V* relations, the presence of divalent cations can lead to an underestimation of the

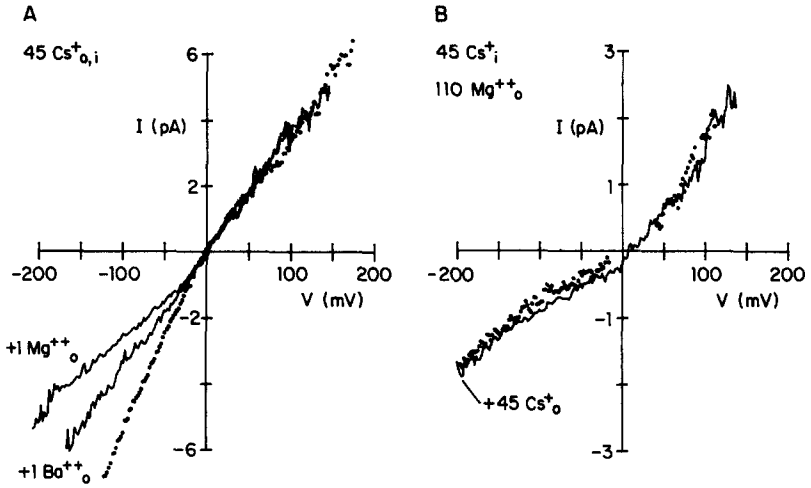

FIGURE 7. (*A*) The dotted *I-V* relation was obtained in pure, symmetrical 45 mM cesium. 1 mM magnesium or barium added to the external solution substantially decreased the inward-going current in a voltage-dependent manner. (*B*) The dotted *I-V* relation was obtained with 45 mM cesium as the internal permeant and 110 mM magnesium as the external permeant. When 45 mM cesium was added to the external 110 mM magnesium solution, the solid *I-V* relation was obtained. These plots indicate that magnesium carries inward-going current, and at high concentrations it largely displaces cesium as the current carrier.

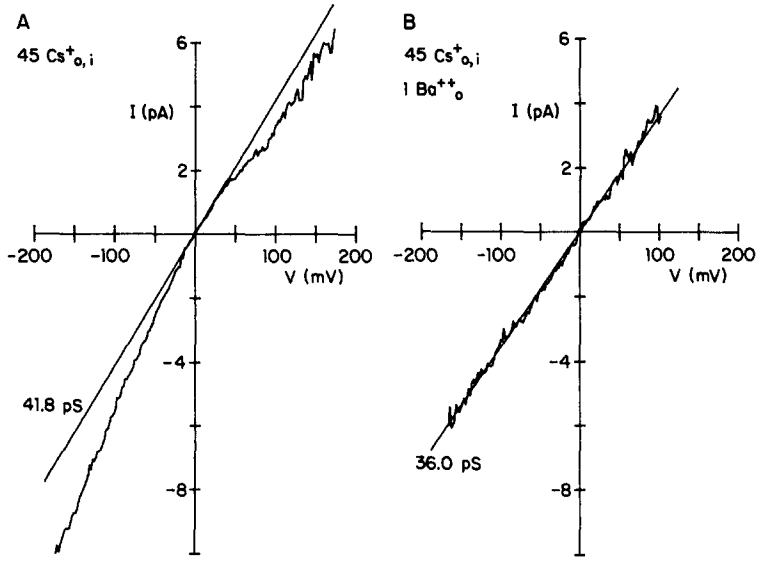

FIGURE 8. (*A*) *I-V* relation obtained in pure, symmetrical 45 mM cesium. The straight line has a slope equal to the zero-voltage conductance, 41.8 pS. (*B*) *I-V* relation obtained after 1 mM barium was added to the external solution. The straight line has a slope equal to the zero-voltage conductance, 36.0 pS. Both the conductance and the shape of the *I-V* were changed by adding only 1 mM barium (or magnesium) to the external solution.

binding affinity of monovalent cations (see Dani, 1986*a*). Because divalent permeants compete with monovalent cations for the binding site within the channel, if this competition is not accounted for, it will appear as though the monovalent cation affinity for the binding site were lower than the true affinity determined in the absence of divalent cations.

The Ion Transport Model

The qualitative features of the data suggest what properties must be accounted for by a quantitative model. Two findings indicate there is at least one binding site for permeant ions within the channel. The single channel conductance begins to level off as the concentration is increased, and permeant ions competitively interfere with each other's transport. Several other findings indicate that some other transport properties besides a single binding site must be considered. The single channel conductance at low concentrations is higher than expected, and divalent ions have a surprisingly high affinity for the channel.

A simple ion transport model with only a few adjustable parameters can only crudely approximate the most important factors involved. The model applied here (Dani, 1986*a*) modifies the simplest reasonable rate theory model to include structural and chemical information about the ACh receptor channel. Since the transport data indicate there is an ion-binding site in the channel, we follow the lead of others by having two barriers separated by one site as the first step toward approximating the energy profile encountered by a permeant cation (Lewis, 1979; Lewis and Stevens, 1979; Marchais and Marty, 1979). Structural studies indicate that the channel has a large outer vestibule and the polypeptide subunits that form the pore do not match up at the cytoplasmic end (Kistler et al., 1982; Brisson and Unwin, 1985). Other evidence suggests there is net negative charge within the channel (Huang et al., 1978), probably in the wide vestibules (Fairclough et al., 1986). The transport model applied here accounts for the size, shape, and the negative potential of the entrance vestibules.

It is supposed that the main determinants of transport are associated with the narrow region of the pore and that the larger vestibules serve as transition zones from the bulk solution to the narrow region. Primarily because of net negatively charged residues making up the walls of the channel, the vestibules provide a "conditioned environment" that influences transport. The negative charge in the channel attracts cations from solution, thus creating in the vestibule a diffuse ionic layer with net positive charge. The net negative charge on the channel walls is screened by the counterions in the electrolyte that are attracted into the vestibule. In that way, the potential in the vestibule caused by the net negative charge varies as a function of the electrolyte concentration. The potential has a more negative value at low electrolyte concentrations. As in Debye-Huckel and Gouy-Chapman theories, an equilibrium between thermal and electrostatic forces leads to an ionic distribution that is dependent (in this case) on the size and shape of the vestibule. This model is physically realistic and, without introducing more adjustable parameters, it automatically describes the higher affinity for divalent cations and the anomalously high single channel conductances seen at low concentrations.

The details of the model and the calculations are given elsewhere (Dani, 1986*a*). Here we give the specific parameters used for the ACh receptor and a brief description of some of the model's properties. A variety of mathematical simplifications are necessary to make the problem tractable: the two-barrier, one-site rate theory model and vestibules are treated separately, all of the potential drop across the membrane occurs in the two-barrier, one-site region, and the vestibules contain one negative charge and are in equilibrium with the bulk solution. To approximate the distribution of positive and negative charges in the channel, the negative charge is placed at the end of each vestibule near the narrow region. The differential equation that gives the diffuse double layer potential is integrated from bulk solution to a position 40% of the way through the vestibule. From that position on, it is assumed that the fluctuating local potential in the vestibule can be approximated by a constant value (see Dani, 1986*a*). It is assumed that 40% of the electric field from the negative charge in each vestibule passes down the pore and into the bulk solution. The rest of the electric field passes into the protein. The outer vestibule is taken to be 6.5 nm long, 2.6 nm wide at its mouth, and 1.2 nm wide just before the narrow region. Because of the difference in the subunits' lengths (Brisson and Unwin, 1985), the cytoplasmic end of the channel is taken to have a vestibule 3.0 nm long, 1.6 nm wide at its mouth, and 1.2 nm wide just before the narrow region. The total potential (V_t) that results in each vestibule is the sum of the negative potential owing to the net negative charge (V_v) and the positive potential owing to the diffuse double layer of ions (V_d). The total potential is always negative, and it affects transport directly in two ways. (*a*) The effective driving force (V_e) for transport of an ion over the two-barrier, one-site profile equals the applied potential (V_a) plus the difference in the total vestibule potentials ($V_e = V_a + V_{ti} - V_{to}$). (*b*) The concentration of each ionic species in the vestibule is related to the bulk concentration by a Boltzmann factor [$C = Cb \exp(zFV_t/RT)$]. It is this concentration in the vestibule that is used in the transport equation of the two-barrier, one-site model.

Comparison of the Model with the Data

In fitting the data with the charged-channel model, only parameters related to the two-barrier, one-site profile were adjusted; none of the vestibule parameters was allowed to vary. The five *I-V* relations obtained with cesium as the permeant were fitted by varying the three energies and their three locations in the two-barrier, one-site profile. All the remaining data sets were fitted by holding the locations fixed at the positions found with cesium and varying only the three energies. We reasoned that the locations of the energy barriers and binding site should be dictated by the channel, and these positions should be roughly the same for all of the small inorganic permeants. The energies were varied for each ionic species to account for differences in the interaction between difference cations and the residues of the channel.

The transport model that includes charged vestibules (called the charged-channel model) describes the cesium and sodium data very well (Fig. 9). Using the same fitting procedure described above, with the same number of adjustable

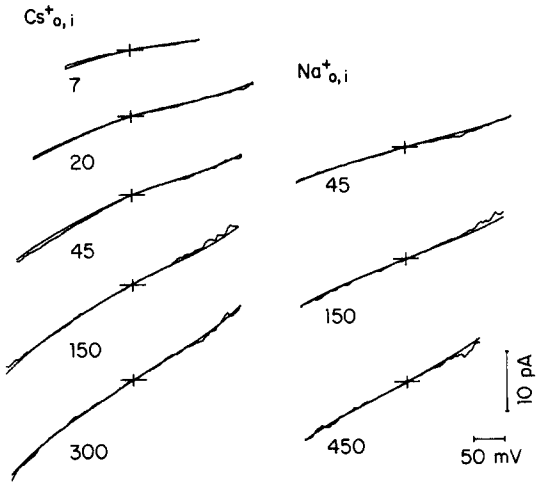

FIGURE 9. The noisy *I-V* relations are cesium and sodium data, and the smooth curves are theoretical fits. The symmetrical concentration of permeant that bathed the patch of membrane labels each *I-V*. The three energies and the three locations of the charged-channel model were adjusted to obtain the fit to the cesium data. The locations were held at the positions found for cesium and only the three energies were adjusted to obtain the fit to the sodium data.

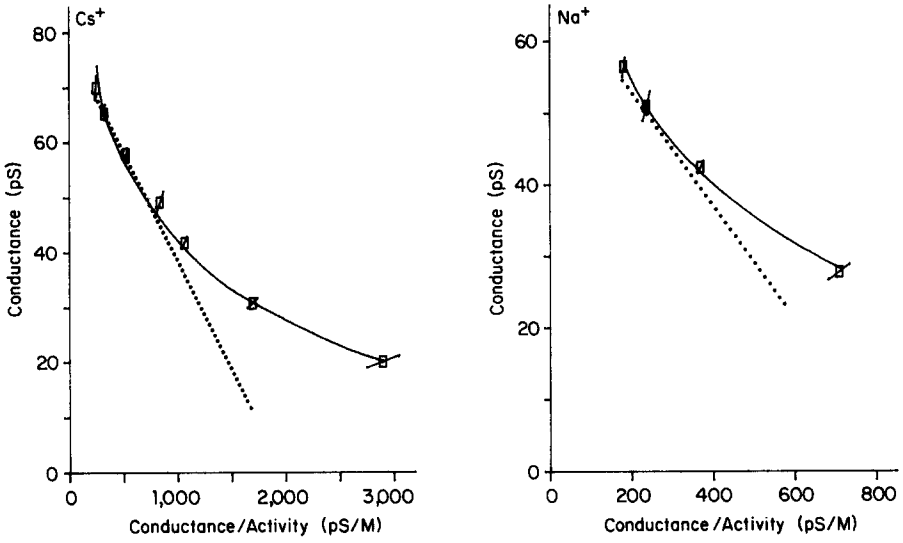

FIGURE 10. Eadie-Hofstee plots of conductance vs. conductance/activity for cesium and sodium. The open squares are data; the solid curves result from the charged-channel model's description of the *I-V* relations; the dotted straight lines result from the simple two-barrier, one-site model's description of the *I-V* relations. Clearly, the unextended two-barrier, one-site model cannot adequately describe the data.

parameters, the simple two-barrier, one-site model without vestibules could not simultaneously describe the cesium and sodium *I-V* relations. The Eadie-Hofstee plot in Fig. 10 points out the success of the charged-channel model over the simple two-barrier, one-site model. The open squares are the zero-voltage conductances determined from the cesium and sodium *I-V* relations. The smooth curves running through the data points were produced by the charged-channel model using the fits in Fig. 9. In contrast, any static two-barrier, one-site model

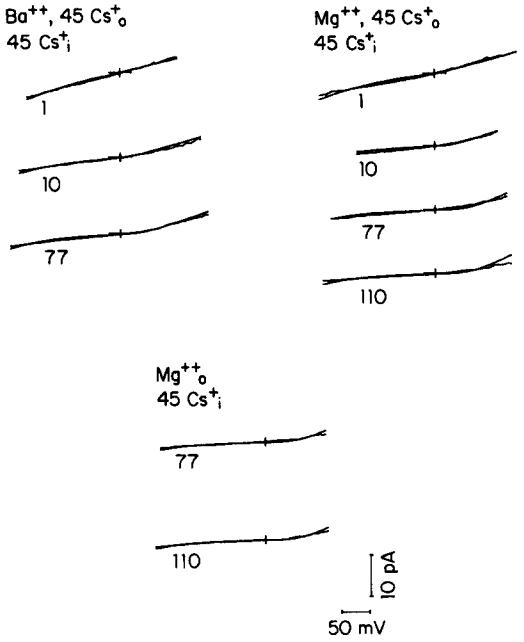

FIGURE 11. The smooth curves are theoretical fits of the charged-channel model to the noisy *I-V* relations obtained with 45 mM cesium bathing the inner surface of the membrane and 45 mM cesium with barium or magnesium bathing the outer surface of the membrane. The lower *I-V*'s were obtained with pure magnesium bathing the outer surface of the membrane. The *I-V* relations are labeled by the concentration of divalent cation that was present in the external solution.

must produce a straight line on an Eadie-Hofstee plot (cf. Eisenman and Dani, 1986) and, clearly, the dotted straight lines predicted by the best two-barrier, one-site fits to the *I-V* data do not describe the data. This qualitative feature of the data is automatically accounted for by the charged-channel model.

The *I-V* relations obtained in the presence of divalent cations were fitted by holding the cesium parameters constant, fixing the locations of the divalent cation's barriers and site at the positions found for cesium, and then adjusting only the three energies for each divalent cation. Fig. 11 shows that the charged-channel model gives good fits to the *I-V* relations obtained with magnesium or barium present. The potential in the vestibules, the energies, and the locations of the barriers and sites are listed in Table II.

TABLE II

Main permeant activity	Outer vestible	Outer barrier	Well	Inner barrier	Inner vestible
mM	*mV*	*KT*	*KT*	*KT*	*mV*
6.9 $Cs_{i,o}$	−60.8	6.352*	−3.886	8.3743	−88.1
18.2 $Cs_{i,o}$	−48.4	"	"	"	−77.0
39.3 $Cs_{i,o}$	−38.6	"	"	"	−65.8
110.6 $Cs_{i,o}$	−25.6	"	"	"	−49.5
200.3 $Cs_{i,o}$	−19.8	"	"	"	−40.2
39.2 $Na_{i,o}$	−35.5	6.850	−3.998	8.442	−62.0
115.0 $Na_{i,o}$	−22.4	"	"	"	−44.4
311.9 $Na_{i,o}$	−13.9		"	"	−29.3
0.9 Mg, 39.2 Cs_o	−36.2	7.749‡	−7.184	10.015	−65.8§
7.5 Mg, 36.0 Cs_o	−28.6	"	"	"	"
43.9 Mg, 30.0 Cs_o	−17.5	"	"	"	"
57.6 Mg, 29.0 Cs_o	−15.7	"	"	"	"
43.9 Mg_o	−18.3	"	"	"	"
57.6 Mg_o	−16.4	"	"	"	"
0.9 Ba, 39.1 Cs_o	−36.7	8.416‡	−6.089	10.736	−65.8§
7.4 Ba, 35.0 Cs_o	−29.7	"	"	"	"
41.6 Ba, 29.0 Cs_o	−19.2	"	"	"	"

The locations (defined as the fraction of the voltage drop to the position) obtained by fitting the cesium data are as follows: outer barrier at 0.1652, site at 0.6198, inner barrier at 0.8041.

* The KT energies are appropriate for a mole fraction equal to 1.0 standard state.

‡ The energies are given for the divalent ion. The energies for cesium are as given above.

§ In the experiments with external divalent cations, the internal solution was always the same. The main permeant activity was 39.3 mM cesium, and the potential in the inner vestibule therefore did not vary.

DISCUSSION

Ion Transport Information

Although the wide portions of the channel contain many ions, it is the occupancy of the narrow region, where the diffusion of the permeant is restricted, that is most important. A variety of different experiments suggests that the ACh receptor channel has primarily one ion-binding site in the narrow portion of the channel. (*a*) The single channel conductance begins to level off at high concentrations, as if a single site were becoming saturated (Fig. 5). (*b*) When sodium was replaced by various organic permeants, the conductance (Sanchez et al., 1986) and the reversal potential (Adams et al., 1980) fell monotonically as a function of the mole fraction of organic permeant. Those findings are consistent with single occupancy. (*c*) The permeability ratio of lithium to ammonium (P_{Li}/P_{NH_4}) was found to have the same value in 10 and 150 mM electrolyte (Dani, 1986*b*; unpublished observation), which is consistent with single occupancy. (*d*) The length of the narrowest portion of the ACh receptor pore has been estimated by determining the number of water molecules coupled to the transport of the largest permeant that can fit through the channel (Dani, 1986*b*, 1987; unpub-

lished observations). Since the narrowest cross section was found to be short, it is likely that only one cation can be present at a time.

There are other features of ion transport that are more difficult to explain. (*a*) The single channel conductance at low concentrations is greater than expected from measurements at high concentrations (curved Eadie-Hofstee plots, Figs. 5 and 10). (*b*) It is known that divalent cations are permeants that reduce the conductance to monovalent cations (Figs. 6 and 7; Bregestovski et al., 1979; Lewis, 1979; Marchais and Marty, 1979; Adams et al., 1980; Magleby and Weinstock, 1980; Takeda et al., 1982). By studying monovalent transport in the absence of divalent cations, we found that divalent cations have a high affinity for the channel and that higher concentrations displace monovalent cations and carry most of the current (Figs. 6 and 7). (*c*) Because divalent and large organic cations (Sanchez et al., 1986) have high affinities for the ACh receptor channel, if their presence is ignored, monovalent cation transport data can be misinterpreted: the *I-V* shape will not reflect the transport of just the small, monovalent permeant, and the apparent affinity of the main permeant will be less than the actual affinity (Fig. 8; also see Dani, 1986*a*). Previously, the monovalent cation *I-V* relations of the ACh receptor have been considered to be ohmic. Here we found that when the divalent cations are removed, the *I-V* relations show some asymmetry and inward rectification at low concentrations (Figs. 4, 8, and 9).

The Charged-Channel Model

In a simple, physically reasonable framework with few adjustable parameters, the charged-channel model provides the properties needed to describe even the complexities in the transport data. Many desired effects follow automatically upon considering the size, shape, and net negative charge of the channel (Dani, 1986*a*). (*a*) The potential caused by the charge in the channel becomes more negative as the bulk electrolyte concentration decreases. This concentration-dependent potential more effectively attracts cations into the channel at low concentrations. This factor explains the high conductances at low permeant concentrations that produce the curved Eadie-Hofstee plots (G vs. G/C; Figs. 5 and 10). (*b*) The potential inside the channel confers selectivity. The negative potential repels anions, which contributes to making the channel cation selective. The charge also contributes to attracting divalent cations more strongly than monovalent cations and is an important factor in the surprisingly high affinity of divalent cations for the channel. (*c*) Size, shape, and possibly charge and binding asymmetry in the vestibules contribute to the asymmetry seen in the transport data.

The value of the charged-channel model can be judged relative to other transport models. No simple, static, one-site rate theory model can describe all the complex features of transport discussed above. Indeed, the complexities are pointed out by the inability of the two-barrier, one-site model to describe the results (Fig. 10). Models with more than one ion-binding site or with fluctuating energy barriers could fit the data by introducing more adjustable parameters. There is no convincing evidence, however, to suggest that either of these possibilities is actually of primary importance. Finally, although the charged-channel model is certainly not correct in its details, it provides a basis for a better

understanding of structural factors that contribute to function at a molecular level. (The exact values of the energies and potentials and the simplifying assumptions of the charged-channel model are not expected to be exactly correct. The underlying principles and the approach, however, seem valid and provide valuable insights. The shortcomings of the charged-channel model are discussed in greater detail elsewhere [Dani, 1986*a*].)

Table II lists the energies associated with the charged-channel model. The potentials in the vestibules depend on the size and shape of the vestibules and the size, charge, and concentration of the electrolyte. The species differences in the two-barrier, one-site energies indicate there is interaction between the permeant and the channel walls.

Selectivity

There are various ways to judge the selectivity of the channel. In a channel that contains only one ion at a time (functionally one main ion-binding site), the permeability that is calculated from the reversal potential is related only to the barrier heights (Hille, 1975; Levitt, 1986). Therefore, on the basis of the barrier heights of the model, the permeability selectivity sequence for the ACh receptor is cesium > sodium and magnesium > barium. Others have determined the permeability selectivity sequence to be cesium > rubidium > potassium > sodium > lithium and magnesium > calcium > barium > strontium (Gage and Van Helden, 1979; Adams et al., 1980; Lewis and Stevens, 1983). Selectivity can also be based on binding affinity and maximum conductance. The model indicates that the affinity for the primary ion-binding site is sodium > cesium and magnesium > barium, and that the maximum conductance is cesium > sodium and barium > magnesium. Estimates of phenomenological values can be made from the conductance plots in Figs. 5 and 10. The maximum conductances can be estimated to be ~80 pS for cesium and ~70 pS for sodium, and the activities for half-maximum conductance are ~40 mM for cesium and ~70 mM for sodium.

Summary Relating Ion Transport to the ACh Receptor Channel

The ACh receptor contains a large water-filled pore that is not very selective. The channel only weakly discriminates among like permeants, and the lyotropic barrier selectivity sequence for alkali cations suggests that a large portion of the channel walls are not lined by high-field-strength charges (Adams et al., 1980). In spite of the water-like environment, evidence indicates that the ACh receptor pore contains charged residues, but probably only a small number. Huang et al. (1978) found that as the pH was lowered, sodium flux was reduced and eliminated, following a simple titration curve with a pK of 4.8. Since agonist binding was little affected at pH 4.75, they concluded that the protonation site was probably within the channel. Consistent with those results, we observed that single channel currents became ~20% smaller when the pH was decreased from 7.4 to 5.0 (unpublished observation). In addition, a negative surface potential has been invoked to explain reversal potential measurements in monovalent-divalent mixtures (Lewis, 1979; Lewis and Stevens, 1979; Adams et al., 1980). Potentials consistent with that view could result from a small amount of negative charge in or near the channel.

There may not, however, be many charged residues within the channel. It has been shown here and elsewhere (Levitt, 1985; Dani, 1986*a*) that one or two charges, even in the wider regions of the channel, have a dramatic effect on ion transport. Although dissimilar charges could be optimally placed to cancel each other, many dissociated charged residues (not screened by hydrogen ions) in the channel would tend to produce large local energy barriers, which are inconsistent with the transport properties. (Although there may be many dissociable side chains lining the channel, it is unlikely that more than a few of these would be charged at physiological pH. Electrostatic attraction of counterions [e.g., hydrogen ions] will suppress the ionization of a group adjacent to one that is already dissociated. The effective pK's of adjacent ionizible groups can be very different from the pK's of the groups when they are alone.) Our data and the crude transport model used here suggest that a small amount of net charge may exist in the wider regions of the pore and possibly at the main ion-binding site. (Many aspects of the concentration-dependent potentials within the channel could arise from the presence of dipolar rather than charged groups.)

Charges in the wider regions would attract counterions, but only a small fraction of ions would form contact pairs with the charged residues caused by statistical (entropic) considerations related to the large free volume (Guggenheim, 1950). Such an arrangement would increase conductance by attracting permeants to the pore without decreasing conductance through strong binding.

Therefore, the large funnel-shaped outer vestibule and a smaller pseudo–inner vestibule formed by the unmatched lengths of the subunits on the cytoplasmic end (Brisson and Unwin, 1985) condition the environment next to the narrower region of the channel. It is likely that each vestibule forms a multiply occupied energy minimum that does not behave like a single site (Dani, 1986*a*). As the cross-sectional area of the pore decreases, the gradient of the potential difference across the membrane becomes steeper and the ions interact more with each other and with the walls of the channel. Our results are consistent with most of the tapering and narrow regions of the pore being lined by dipoles, not by many charged residues. In addition, apolar side chains may come together to produce some hydrophobic interactions within the pore (Adams et al., 1981; Farley et al., 1981). The narrowest portion of the channel, located near the cytoplasmic end of the channel (Brisson and Unwin, 1985), is short and singly occupied (Dani, 1986*b*, 1987; unpublished observations). This is the place where the channel most intimately interacts with the permeant to produce a legitimate binding site and possibly energy barriers. Friction between the permeant and water and the channel walls, partial dehydration, long-distance diffusion, and binding at the narrowest region may limit transport more than large energy barriers caused by strong chemical interactions throughout the length of the pore.

Biological Importance

The ultimate goal of relating structure and function may be achieved through a long series of experiments with site-directed mutagenesis (Mishina et al., 1985). The transport information presented here should serve as a basis for judging particular mutations to probe the permeation pathway. Structural models for

the ACh receptor channel have been proposed on the basis of the complete amino acid sequences of the cloned subunits (Ballivet et al., 1982; Noda et al., 1982, 1983; Claudio et al., 1983; Devillers-Thiery et al., 1983). It is proposed that the subunits are arranged like staves of a barrel around a central pore, with each subunit contributing an α-helix to form the walls. The structural models that have not been eliminated (see Stevens, 1985) include those that propose that rings of negative and positive charge line the membrane-spanning region of the pore (Guy, 1984; Finer-Moore, 1984; Ratnam et al., 1986). Although these models suggest there is little net charge, rings of dissociated charges in the tapering and narrow portion of the pore would produce transport barriers and sites that would be too severe to explain our results (see Levitt, 1985; Dani, 1986*a*). Therefore, we suggest that the uncharged membrane-spanning regions of the primary sequences called M1 or M2 (see Noda et al., 1983) are more likely candidates for the α-helix that forms the lining of the pore, rather than the highly charged α-helixes, M5 (Guy, 1984; Finer-Moore and Stroud, 1984) or M7 (Ratnam et al., 1986). The M1 membrane-spanning region has strategically located, conserved proline residues. Proline residues break the α-helix structure, exposing carbonyl dipoles, which could then serve to coordinate an ion in a binding site (see Eisenman and Dani, 1987). M2 is also an appealing candidate because it has excess negative charge bracketing the membrane-spanning regions, as suggested by our data and by the charged-channel transport model. Recently, Imoto et al. (1986) have presented evidence that M2 and the adjacent segment between α-helix M2 and M3 influence ion transport. (See Noda et al., 1983, for the amino acid sequences of the membrane-spanning regions.)

This work also shows that physiologic concentrations of divalent ions modulate monovalent transport, and the divalent cations are transported with surprising efficiency. At nicotinic synapses, the ACh receptors are packed very densely, with as many as 20,000 receptors per square micrometer at the top of the junctional folds (Matthews-Bellinger and Salpeter, 1978). Therefore, the ionic environment beneath the endplate is a unique product of the electrical activity of the synapse. The involvement of divalent cations in the regulation and modification of cellular processes is well known. Thus, ion transport through the ACh receptor may be expected to serve other important roles at the postsynaptic endplate besides depolarizing the cell.

We gratefully acknowledge Ms. Lis Greene for assistance with the tissue culture.

This work was supported by the National Science Foundation (BNS 84-11033) and the U.S. Public Health Service (GM-24749 and New Investigator Research Award NS-21229).

Original version received 5 September 1986 and accepted version received 5 February 1987.

REFERENCES

Adams, D. J., T. M. Dwyer, and B. Hille. 1980. The permeability of end-plate channels to monovalent and divalent metal cations. *Journal of General Physiology.* 75:493–510.

Adams, D. J., W. Nonner, T. M. Dwyer, and B. Hille. 1981. Block of endplate channels by permeant cations in skeletal muscle. *Journal of General Physiology.* 78:593–615.

Andersen, O. S. 1983. Ion movement through gramicidin A channels: studies on the diffusion-controlled association step. *Biophysical Journal.* 41:147–165.

Apell, H. J., E. Bamberg, and P. Lauger. 1979. Effects of surface charge on the conductance of the gramicidin channel. *Biochimica et Biophysica Acta.* 552:369–378.

Ballivet, M., J. Patrick, and S. Heinemann. 1982. Molecular cloning of cDNA coding for the subunit of *Torpedo* acetylcholine receptor. *Proceedings of the National Academy of Sciences.* 79:4466–4470.

Bell, J. E., and C. Miller. 1984. Effects of phospholipid surface charge on ion conduction in the K^+ channel of sarcoplasmic reticulum. *Biophysical Journal.* 45:279–288.

Bregestovski, P. D., R. Miledi, and I. Parker. 1979. Calcium conductance of acetylcholine induced end-plate channels. *Nature.* 279:638–639.

Brisson, A., and P. N. T. Unwin. 1985. Quaternary structure of the acetylcholine receptor. *Nature.* 315:474–477.

Claudio, T., M. Ballivet, J. Patrick, and S. Heinemann. 1983. Nucleotide and deduced amino acid sequences of *Torpedo californica* acetylcholine receptor subunit. *Proceedings of the National Academy of Sciences.* 80:1111–1115.

Cooper, K., E. Jakobsson, and P. Wolynes. 1985. The theory of ion transport through membrane channels. *Progress in Biophysics and Molecular Biology.* 46:51–96.

Dani, J. A. 1986*a*. Ion-channel entrances influence permeation: net charge, size, shape, and binding considerations. *Biophysical Journal.* 49:607–618.

Dani, J. A. 1986*b*. Inferred internal structure of the acetylcholine receptor pore. *Neuroscience Abstracts.* 12:1510.

Dani, J. A. 1987. Streaming potential measurements indicate the narrowest cross section of the nicotinic acetylcholine receptor pore is very short. *Biophysical Journal.* 51:395*a*. (Abstr.)

Dani, J. A., and G. Eisenman. 1984. Acetylcholine-activated channel current-voltage relations in symmetrical Na^+ solutions. *Biophysical Journal.* 45:10–12.

Dani, J. A., and G. Eisenman. 1985. Acetylcholine receptor channel permeability properties for mono- and divalent cations. *Biophysical Journal.* 47:43*a*. (Abstr.)

Devillers-Thiery, A., J. Giraudat, M. Bentaboulet, and J.-P. Changeux. 1983. Complete mRNA coding sequence of the acetylcholine binding α-subunit of *Torpedo marmorata* acetylcholine receptor: a model for the transmembrane organization of the polypeptide chain. *Proceedings of the National Academy of Sciences.* 80:2067–2071.

Dwyer, T. M., D. J. Adams, and B. Hille. 1980. The permeability of end-plate channels to organic cations in frog muscle. *Journal of General Physiology.* 75:469–492.

Dwyer, T. M., and J. M. Farley. 1984. Permeability properties of chick myotube acetylcholine-activated channels. *Biophysical Journal.* 45:529–539.

Eisenman, G., and J. A. Dani. 1986. Characterizing the electrical behavior of an open channel via the energy profile for ion permeation: a prototype using a fluctuating barrier model for the acetylcholine receptor channel. *In* Ionic Channels in Cells and Model Systems. R. Latorre, editor. Plenum Publishing Corp., New York. 53–87.

Eisenman, G., and J. A. Dani. 1987. An introduction to molecular architecture and permeability of ionic channels. *Annual Review of Biophysics and Biophysical Chemistry.* 16:205–226.

Eisenman, G., R. Latorre, and C. Miller. 1986. Multi-ion conduction and selectivity in the high-conductance Ca^{++}-activated K^+ channel from skeletal muscle. *Biophysical Journal.* 50:1025–1034.

Eisenman, G., J. Sandblom, and E. Neher. 1978. Interactions in cation permeation through the gramicidin channel: Cs, Rb, K, Na, Li, Tl, H, and effects of anion binding. *Biophysical Journal.* 22:307–340.

Fairclough, R. H., R. C. Miake-Lye, R. M. Stroud, K. O. Hodgson, and S. Doniach. 1986. Location of terbium binding sites on acetylcholine receptor-enriched membranes. *Journal of Molecular Biology.* 189:673–680.

Farley, J. M., J. Z. Yeh, S. Watanabe, and T. Narahashi. 1981. Endplate channel block by guanidine derivatives. *Journal of General Physiology.* 77:273–293.

Finer-Moore, J., and R. M. Stroud. 1984. Amphipathic analysis and possible formation of the ion channel in an acetylcholine receptor. *Proceedings of the National Academy of Sciences.* 81:155–159.

Gage, P. W., and D. F. Van Helden. 1979. Effects of permeant monovalent cations on endplate channels. *Journal of Physiology.* 288:509–528.

Guggenheim, E. A. 1950. Thermodynamics. North Holland Publishing Co., Amsterdam.

Guy, H. R. 1984. A structural model of the acetylcholine receptor channel based on partition energy and helix packing calculations. *Biophysical Journal.* 45:249–261.

Hamill, O. P., A. Marty, E. Neher, B. Sakmann, and F. J. Sigworth. 1981. Improved patch-clamp techniques for high-resolution current recordings from cells and cell-free membrane patches. *Pflügers Archiv.* 391:85–100.

Hille, B. 1975. Ionic selectivity of Na and K channels of nerve membranes. *In* Membranes: a Series of Advances. Lipid Bilayers and Biological Membranes: Dynamic Properties. G. Eisenman, editor. Marcel Dekker, New York. 3:255–323.

Hille, B., and W. Schwarz. 1978. Potassium channels as multi-ion single-file pores. *Journal of General Physiology.* 72:409–442.

Huang, L. M., W. A. Catterall, and G. Ehrenstein. 1978. Selectivity of cations and nonelectrolytes for acetylcholine-activated channels in cultured muscle cells. *Journal of General Physiology.* 71:397–410.

Imoto, K., C. Methfessel, B. Sakmann, M. Mishina, Y. Mori, T. Konno, K. Fukuda, M. Kurasaki, H. Bujo, Y. Fujita, and S. Numa. 1986. Location of the γ-subunit region determining ion transport through the acetylcholine receptor channel. *Nature.* 324:670–674.

Kistler, J., R. M. Stroud, M. W. Klymkowski, R. A. Lalancette, and R. H. Fairclough. 1982. Structure and function of an acetylcholine receptor. *Biophysical Journal.* 37:371–383.

Lauger, P., W. Stephan, and E. Frehland. 1980. Fluctuation of barrier structure in ionic channels. *Biochimica et Biophysica Acta.* 602:167–180.

Levitt, D. G. 1985. Strong electrolyte continuum theory solution for equilibrium profiles, diffusion limitation, and conductance in charged ion channels. *Biophysical Journal.* 48:19–31.

Levitt, D. G. 1986. Interpretation of biological ion channel flux data: reaction-rate versus continuum theory. *Annual Reviews of Biophysics and Biophysical Chemistry.* 15:29–57.

Lewis, C. A. 1979. Ion-concentration dependence of the reversal potential and the single channel conductance of ion channels at the frog neuromuscular junction. *Journal of Physiology.* 286:417–455.

Lewis, C. A., and C. F. Stevens. 1979. Mechanism of ion permeation through channels in a postsynaptic membrane. *In* Membrane Transport Processes. C. F. Stevens and R. W. Tsien, editors. Raven Press, New York. 3:89–103.

Lewis, C. A., and C. F. Stevens. 1983. Acetylcholine receptor channel ionic selectivity: ions experience an aqueous environment. *Proceedings of the National Academy of Sciences.* 80:6110–6113.

Mackay, D. H. J., P. H. Berens, K. R. Wilson, and A. T. Hagler. 1984. Structure and dynamics of ion transport through gramicidin A. *Biophysical Journal.* 46:229–248.

Magleby, K. L., and M. M. Weinstock. 1980. Nickel and calcium ions modify the characteristics of the acetylcholine receptor-channel complex at the frog neuromuscular junction. *Journal of Physiology.* 299:203–218.

Marchais, D., and A. Marty. 1979. Interaction of permeant ions with channels activated by acetylcholine in *Aplysia* neurones. *Journal of Physiology.* 297:9–45.

Matthews-Bellinger, J., and M. M. Salpeter. 1978. Distribution of acetylcholine receptors at frog neuromuscular junctions with a discussion of some physiological implications. *Journal of Physiology.* 279:197–213.

Mishina, M., T. Tobimatsu, K. Imoto, K. Tanaka, Y. Fujita, K. Fukuda, M. Kurasaki, H. Takahashi, Y. Morimoto, T. Hirose, S. Inayama, T. Takahashi, M. Kuno, and S. Numa. 1985. Location of functional regions of acetylcholine receptor alpha-subunit by site-directed mutagenesis. *Nature.* 313:364–369.

Noda, M., H. Takahashi, T. Tanabe, M. Toyosato, Y. Furutani, T. Hirose, M. Asai, S. Inayama, T. Miyata, and S. Numa. 1982. Primary structure of α-subunit precursor of *Torpedo californica* acetylcholine receptor deduced from cDNA sequence. *Nature.* 299:793–797.

Noda, M., H. Takahashi, T. Tanabe, M. Toyosato, S. Kikyotani, Y. Furutani, T. Hirose, H. Takashima, S. Inayama, T. Miyata, and S. Numa. 1983. Structural homology of *Torpedo californica* acetylcholine receptor subunits. *Nature.* 302:528–532.

Rae, J. L., and R. A. Levis. 1984. Patch clamp recordings from the epithelium of the lens obtained using glasses selected for low noise and improved sealing properties. *Biophysical Journal.* 45:144–146.

Ratnam, M., D. Le Nguyen, J. Rivier, P. B. Sargent, and J. Lindstrom. 1986. Transmembrane topography of nicotinic acetylcholine receptor: immunochemical tests contradict theoretical predictions based on hydrophobicity profiles. *Biochemistry.* 25:2633–2643.

Robinson, R. A., and R. H. Stokes. 1965. Electrolyte Solutions. 2nd edition. Butterworths, London. 465 pp.

Sakmann, B., and E. Neher, editors. 1983. Single-Channel Recording. Plenum Publishing Corp., New York. 503 pp.

Sanchez, J. A., J. A. Dani, D. Siemen, and B. Hille. 1986. Slow permeation of organic cations in acetylcholine receptor channels. *Journal of General Physiology.* 87:985–1001.

Stevens, C. F. 1985. AChR structure: a new twist in the story. *Trends in Neuroscience.* 8:1–2.

Takeda, K., P. W. Gage, and P. H. Barry. 1982. Effects of divalent cations on toad end-plate channels. *Journal of Membrane Biology.* 64:55–66.

Takeuchi, A., and N. Takeuchi. 1960. On the permeability of end-plate membrane during the action of transmitter. *Journal of Physiology.* 154:52–67.

Weast, R. C., and M. J. Astle. 1978–1979. CRC Handbook of Chemistry and Physics. CRC Press, Inc., Boca Raton, FL.

Yellen, G. 1984. Ionic permeation and blockade in Ca^{2+}-activated K^+ channels of bovine chromaffin cells. *Journal of General Physiology.* 84:157–186.